Available online at www.sciencedirect.com
ScienceDirect
Journal of Solid State Chemistry 180 (2007) 1582–1589
JOURNAL OF SOLID STATE CHEMISTRY
www.elsevier.com/locate/jssc

Preparation, crystal structure and magnetic behavior of new double perovskites $Sr_2B'UO_6$ with $B' = Mn$, Fe, Ni, Zn

R.M. Pinacca[a], M.C. Viola[a], J.C. Pedregosa[a], M.J. Martínez-Lope[b], R.E. Carbonio[c], J.A. Alonso[b,*]

[a]*Area de Química General e Inorgánica "Dr. Gabino F. Puelles", Departamento de Química, Facultad de Química, Bioquímica y Farmacia, Universidad Nacional de San Luis, Chacabuco y Pedernera, 5700-San Luis, Argentina*
[b]*Instituto de Ciencias de Materiales de Madrid, CSIC, Cantoblanco, E-28049 Madrid, Spain*
[c]*INFIQC, Departamento de Físicoquímica, Facultad de Ciencias Químicas, Universidad Nacional de Córdoba, Ciudad Universitaria, 5000 Córdoba, Argentina*

Received 9 February 2007; received in revised form 28 February 2007; accepted 5 March 2007
Available online 12 March 2007

Abstract

$Sr_2B'UO_6$ double perovskites with $B' = Mn$, Fe, Ni, Zn have been prepared in polycrystalline form by solid-state reaction, in air or reducing conditions. These new materials have been studied by X-ray diffraction (XRD), magnetic susceptibility and magnetization measurements. The room-temperature crystal structure is monoclinic (space group $P2_1/n$), and contains alternating $B'O_6$ and UO_6 octahedra sharing corners, tilted along the three pseudocubic axes according to the Glazer notation $a^-a^-b^+$. The magnetic measurements show a spontaneous magnetic ordering below $T_N = 21$ K for $B' = Mn$, Ni, and $T_C = 150$ K for $B' = Fe$. From a Curie–Weiss fit, the effective paramagnetic moment for $B' = Mn$ (5.74 μ_B/f.u.) and $B' = Ni$(3.51 μ_B/f.u.) are significantly different from the corresponding spin-only moments for the divalent cations, suggesting the possibility of a partial charge disproportionation $B'^{2+} + U^{6+} \Leftrightarrow B'^{3+} + U^{5+}$, also accounting for plausible ferrimagnetic interactions between B' and U sublattices. The strong curvature of the reciprocal susceptibility for $B' = Fe$ precludes a Curie–Weiss fit but also suggests the presence of ferrimagnetic interactions in this compound. This charge disproportionation effect is also supported by the observed B'–O distances, which are closer to the expected values for high-spin, trivalent Mn, Fe and Ni cations.

Keywords: Double perovskite; Crystal structure; Charge disproportionation; Ferrimagnetism; Uranium; X-ray powder diffraction; Rietveld refinement

1. Introduction

When the intrinsic tunneling-type magneto-resistance (MR) phenomenon was discovered in the double perovskite Sr_2FeMoO_6 at room temperature, solid state chemists and physicists became interested in obtaining other substituted phases of stoichiometry $A_2B'B''O_6$ (A = alkali earths, B', B'' = transition metals), since this effect is of technological interest for the detection of magnetic fields in magnetic memory devices [1,2]. In the paradigmatic Sr_2FeMoO_6 oxide the B positions of the perovskite structure are occupied alternately by Fe and Mo atoms, in such a way that each FeO_6 octahedron is corner-linked to six MoO_6 octahedra and vice versa in an ordered array. The magnetic structure was described as an ordered arrangement of parallel Fe^{3+} ($3d^5$, $S = \frac{5}{2}$) magnetic moments antiferromagnetically coupled with Mo^{5+} ($4d^1$, $S = \frac{1}{2}$) spins [3]. The itinerant character of the down-spin Mo electron is in the origin of both ferromagnetic and halfmetallic behavior of this material.

Further studies on other members of the $A_2B'B''O_6$ family seem to indicate that the occurrence of MR properties is a common feature in some of them. Thus, large intragrain (bulk) MR above room temperature has been described in double perovskites with different A cations, such as Ba_2FeMoO_6 [4] or Ca_2FeMoO_6 [5], or different B'' second and third-row transition metals like Sr_2FeReO_6 [6]. Also, MR properties have been described

*Corresponding author. Fax: +34 91 372 06 23.
E-mail address: ja.alonso@icmm.csic.es (J.A. Alonso).

0022-4596/$ - see front matter © 2007 Elsevier Inc. All rights reserved.
doi:10.1016/j.jssc.2007.03.002

for double perovskites with B' cations other than Fe, like in the phase Sr_2CoMoO_6 after topotactic removal of oxygen atoms [7].

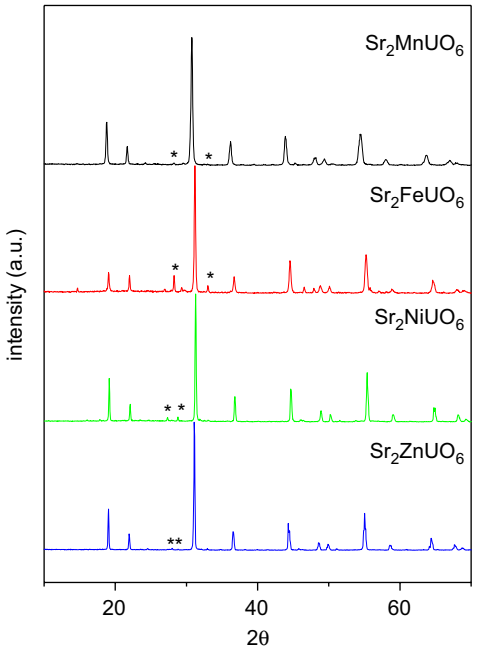

Fig. 1. XRD patterns of $Sr_2B'UO_6$. The stars correspond to the most intense reflections of the minor impurities $SrUO_4$ (B' = Mn, Fe, Zn) or Sr_2UO_5 (B' = Ni).

It is remarkable that most of the studies on double perovskites with B' = Cr, Mn, Fe, Co, Ni have been performed on materials containing Mo, Re, W or Te as B'' cations [8–21], but very little work has been done on uranium-containing double perovskites (B'' = U) [22–25], most of the reported phases containing Ba as A cation. Both hexavalent uranium or pentavalent uranium could exist in this structural type when B' is a divalent or trivalent first-row transition metal. We focused our attention on the uranium analogs of the mentioned families and recently we prepared and studied the Sr_2CoUO_6 double perovskite, for which we determined the crystal and magnetic structures from neutron powder diffraction data (NPD) [26]. This compound presents a subtle monoclinic distortion at RT and a canted antiferromagnetic structure is observed below $T_N = 10$ K.

As a continuation of this investigation, we have prepared and characterized the new double perovskites $Sr_2B'UO_6$ with B' = Mn, Fe, Ni, Zn; in this paper we report on the results of an X-ray diffraction (XRD) structural study, complemented with macroscopic magnetic measurements.

2. Experimental

The $Sr_2B'UO_6$ phases for B' = Ni, Zn were synthesized by the standard ceramic method. These compounds were prepared as black and yellow polycrystalline powders (Ni and Zn, respectively) by solid state reaction of

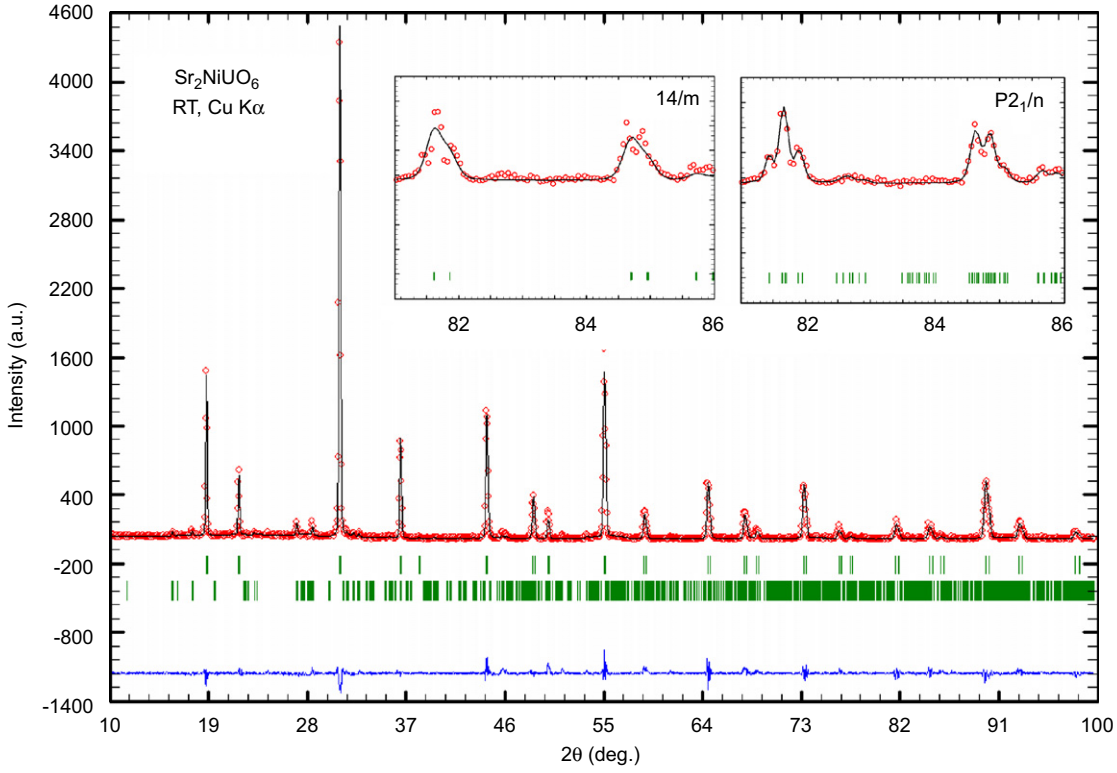

Fig. 2. Observed (crosses), calculated (solid line) and difference (bottom line) XRD patterns corresponding to the refinement of the Sr_2NiUO_6 crystallographic structure at RT. The second series of tick marks correspond to the Sr_2UO_5 impurity. The two insets show a close up the poor fit in $I/4m$ and the satisfactory refinement in $P2_1/n$ in a selected angular region between 81° and 86°.

stoichiometric amounts of analytical grade $SrCO_3$, $B'CO_3$ and $UO_2(CH_3COO)_2$. The reactants were mixed, ground, placed in a platinum crucible and treated at 600 °C in air for 12 h and the resulting powder was reground and calcined at 900 °C for 12 h. Finally the product was fired at 1150 °C in air in four periods totaling 24 h with intermediate milling of the reaction mixture. For the $Sr_2B'UO_6$ phases with $B' = Mn$ and Fe the citrate-precursor method was used. The corresponding carbonates/acetates were dissolved in citric acid with formation of a resin which was decomposed at 700 °C in air. The precursor powders underwent a subsequent heating at 800 °C in air. Finally, the products were fired at 950 °C during 6 h in reducing atmosphere (1% H_2 + 99% Ar) in order to stabilize the Fe^{2+} and Mn^{2+} cations.

The characterization by XRD was performed using a Bruker-axs D8 diffractometer (40 kV, 30 mA), controlled by a DIFFRACTplus software, in Bragg-Brentano reflection geometry with CuK_α radiation ($\lambda = 1.5418$ Å). A secondary graphite monochromator allowed the complete removal of CuK_β radiation. The data were obtained between 10° and 100° 2θ in steps of 0.05°. The slit system was selected to ensure that the X-ray beam was completely within the sample for all 2θ angles. The refinement of the crystal structure was performed by the Rietveld method [27] using the FULLPROF program [28]. A pseudo-Voigt function was chosen to generate the line shape of the diffraction peaks. No regions were excluded in the refinements. In the final run the following parameters were refined: scale factors, zero-point, background coefficients, pseudo-Voigt and peak width corrected for asymmetry parameters, positional coordinates and unit-cell parameters. Isotropic thermal factors were set to 0.3 and 0.7 Å^2 for metals and oxygen atoms, respectively, and an overall thermal factor was also refined.

The magnetic measurements were performed in a commercial superconducting quantum interference device magnetometer (SQUID). The susceptibility was measured in field cooling conditions under a 1 kOe magnetic field, for temperatures ranging from $T = 5$ to 400 K. Isothermal magnetization curves were obtained at $T = 5$ K under an applied magnetic field that varied in the ± 50 kOe range.

3. Results and discussion

3.1. Crystal structure

$Sr_2B'UO_6$ with $B' =$ Mn, Fe, Ni, Zn were obtained as well crystallized powders; Fig. 1 shows the corresponding XRD diagrams. Minor amounts of impurities were detected from XRD data; $SrUO_4$ was identified for $B' =$ Mn, Fe and Zn, and Sr_2UO_5 for $B' =$ Ni; the most intense reflections of the impurities are indicated with stars in each diagram. The double-perovskite patterns can be indexed in a monoclinic unit cell with lattice parameters related to a_0 (ideal cubic perovskite, $a_0 \approx 3.8$ Å) as $a \approx \sqrt{2}a_0$, $b \approx \sqrt{2}a_0$, $c \approx 2a_0$, $\beta \approx 90°$. The relatively intense superstructure peaks (0 1 1) and (0 1 3) correspond to the long-range B'/U ordering over the B positions. In $P2_1/n$ it is necessary to define two crystallographically independent B positions (B' and U), as well as 3 kinds of non-equivalent oxygen atoms (O1, O2 and O3), all in general (x,y,z) positions. This is the symmetry and space group adopted by other related Sr or Ca double perovskites, such as Sr_2CoUO_6 [26] or Ca_2FeMoO_6 [5]. The Goldschmidt tolerance factor, defined as $t = (A\text{–O})/\sqrt{2}(B\text{–O})$, equals to unity for the ideal cubic aristotype and becomes lower than unity as the A cation size decreases or the B-size increases, leading to reductions from the cubic symmetry to tetragonal, orthorhombic or monoclinic symmetry due to the progressive tilting of the BO_6 octahedra. In the present case, the large size of U^{6+}/U^{5+} cations at the B positions justifies the reduction of the tolerance factor and symmetry with respect to other well-known Sr perovskites exhibiting tetragonal ($I4/m$) symmetry (for instance the paradigmatic Sr_2FeMoO_6 at RT). Usually, the difference in symmetry is extremely subtle, since it mainly arises from the shift of some O atoms, and it is only unveiled from a careful neutron diffraction study. In the present case, an initial refinement of the crystal structure of the four compounds in the standard tetragonal $I4/m$ model, characterized by

Table 1
Structural parameters for $Sr_2B'UO_6$ ($B' =$ Mn, Fe, Ni, Zn) in the monoclinic $P2_1/n$ space group after the Rietveld refinement of XRD data at RT

B'	Mn	Fe	Ni	Zn
a (Å)	5.8968(8)	5.7990(9)	5.7809(3)	5.8320(4)
b (Å)	5.8537(8)	5.7819(9)	5.7752(3)	5.8119(4)
c (Å)	8.278(1)	8.167(1)	8.1562(5)	8.2004(6)
V (Å)^3	285.75(7)	273.8(3)	272.3(3)	277.95(4)
β	90.014(8)	89.829(3)	89.8370(7)	89.958(2)
Sr 4e(x,y,z)				
x	0.975(1)	0.985(3)	0.995(2)	1.023(1)
y	0.0294(9)	0.018(2)	0.0255(8)	0.0267(9)
z	0.251(2)	0.264(2)	0.235(1)	0.242(1)
B' 2d(1/2,0,0)				
U 2c(1/2,0,1/2)				
O1 4e(x,y,z)				
x	0.012(16)	0.099(9)	0.076(12)	0.052(10)
y	0.480(6)	0.488(10)	0.489(6)	0.500(6)
z	0.239(7)	0.229(5)	0.245(7)	0.249(6)
O2 4e(x,y,z)				
x	0.744(109	0.745(13)	0.731(13)	0.674(9)
y	0.276(10)	0.294(12)	0.290(12)	0.336(10)
z	0.042(9)	0.048(12)	0.047(9)	0.027(9)
O3 4e(x,y,z)				
x	0.152(10)	0.242(13)	0.231(13)	0.239(10)
y	0.161(11)	0.238(11)	0.237(12)	0.232(10)
z	0.963(8)	0.960(12)	0.967(10)	0.957(8)
Reliability factors				
χ^2	1.52	1.75	1.38	1.87
R_I (%)	4.53	5.61	4.61	4.58

a single antiphase tilting along the *c*-axis, yielded reasonable fits to the XRD data, but a careful examination of certain regions of the XRD patterns unequivocally showed the need to introduce a reduction in symmetry. As an illustration, the inset of Fig. 2 shows a close-up of a region of the diagram of the B' = Ni pattern, temptatively refined in $I4/m$, displaying a poor fit to the splitting of certain reflections; the fit was substantially improved by considering the $P2_1/n$ space group where the mentioned splitting is taken into account.

The ideal monoclinic model corresponds to an ordered double perovskite where B' and U occupy different crystallographic sites, with distinct oxygen environments. The refinement of the level of anti-site defects (B' at U sites, and vice versa) allowed us to evaluate the degree of long-range ordering as 91.2% (B' = Mn); 71.6% (B' = Fe); 95.6% (B' = Ni) and 100% (B' = Zn). $SrUO_4$ and Sr_2UO_5 were included as secondary phases in the final refinements. $SrUO_4$ is rhombohedral (space group R–3 m) and Sr_2UO_5 is monoclinic (space group $P2_1/c$). From the scale factors of the main and secondary phases, we estimated 0.27% of $SrUO_4$ in Sr_2MnUO_6; 9.7% of $SrUO_4$ in Sr_2FeUO_6; 5.56% of Sr_2UO_5 in Sr_2NiUO_6 and 0.21% of $SrUO_4$ in Sr_2ZnUO_6. After the final refinement we obtained reasonable reliability factors, included in Table 1, together with the final unit-cell and atomic parameters. The monoclinic beta angles are very close to 90°, indicating a strong pseudo-orthorhombic character of the unit cells. An example of the good agreement between the observed and calculated patterns after the refinements is illustrated in Fig. 2 for B' = Ni; for the remaining phases similar fits were obtained. The mean interatomic distances and some selected bond angles are listed in Table 2.

The perovskite structure contains alternating $B'O_6$ and UO_6 octahedra, displaying an in-phase octahedra tilting along the (001) direction of the pseudocubic cell, and an antiphase along the (100) and (010) directions (see Fig. 3), which corresponds to the $a^-a^-b^+$ Glazer's notation as derived by Woodward [29] for 1:1 ordering in double perovskites, consistent with space group $P2_1/n$. The magnitude of the tilting can be simply derived from the average $\langle B'\text{–O–}U \rangle$ angle, yielding 12.5° (Mn, Fe and Zn), and 11° (Ni). For the sake of comparison, the previously reported Sr_2CoUO_6 oxide [26], belonging to the same $Sr_2B'UO_6$ family, also showed a subtle monoclinic distortion driven by an average tilting of the CoO_6 and UO_6 octahedra by 11.4°.

Whereas the $\langle$ Zn–O $\rangle$ average distance (2.11 Å, Table 2) is in reasonable agreement with the expected value from the ionic radii sums [30] for divalent and hexacoordinated

Table 2
Main bond distances (Å) and selected angles (°) for $Sr_2B'UO_6$ (B' = Mn, Fe, Ni, Zn) determined from XRD data at RT

B'	Mn	Fe	Ni	Zn
SrO_9 *polyhedra*				
Sr–O1	3.04(10)	3.15(4)	3.13(4)	3.06(3)
Sr–O1	2.89(10)	2.81(6)	2.72(4)	2.76(3)
Sr–O1	2.65(3)	2.42(6)	2.49(7)	2.48(6)
Sr–O2	2.63(7)	2.76(9)	2.65(7)	2.61(7)
Sr–O2	2.60(7)	2.40(9)	2.59(7)	2.48(7)
Sr–O2	3.10(7)	2.97(9)	3.08(8)	3.25(6)
Sr–O3	2.71(6)	3.16(9)	2.85(8)	2.92(7)
Sr–O3	3.16(6)	2.55(8)	2.79(8)	2.79(6)
Sr–O3	2.22(6)	2.70(8)	2.60(8)	2.70(6)
$\langle$ Sr–O $\rangle$	$2.62(7)_{6short}$	$2.66(8)_{7short}$	$2.67(7)_{7short}$	$2.68(6)_{7short}$
$B'O_6$ *octahedra*				
B'–O1 ($x2$)	1.99(6)	1.96(5)	2.05(6)	2.07(5)
B'–O2 ($x2$)	2.03(6)	1.94(7)	2.01(7)	2.14(6)
B'–O3 ($x2$)	2.20(6)	2.09(7)	2.04(7)	2.12(6)
$\langle B'\text{–O} \rangle$	2.07(6)	2.00(6)	2.03(7)	2.11(6)
UO_6 *Octahedra*				
U–O1 ($x2$)	2.16(6)	2.28(5)	2.13(6)	2.08(7)
U–O2 ($x2$)	2.19(6)	2.25(7)	2.18(7)	2.21(6)
U–O3($x2$)	2.28(6)	2.06(7)	2.09(7)	2.06(6)
$\langle U\text{–O} \rangle$	2.18(6)	2.1(1)	2.13(7)	2.12(6)
U–O1–B'	172(2)	148(2)	155(2)	163(2)
U–O2–B'	159(2)	155(3)	155(3)	142(2)
U–O3–B'	136(2)	161(3)	164(3)	159(2)
$\langle U\text{–O}\text{–}B' \rangle$	155(2)	155(2)	158(3)	155(2)

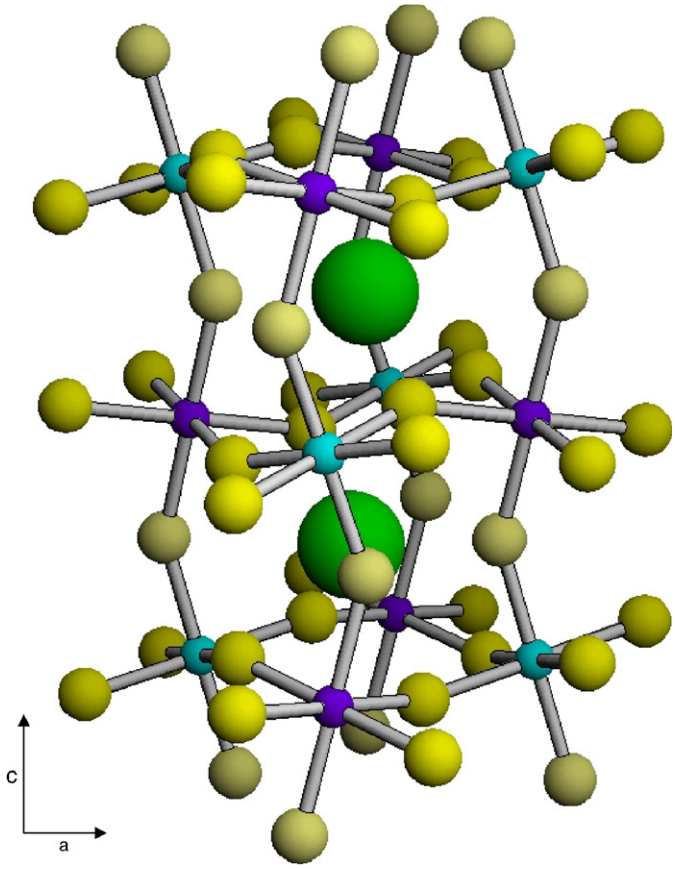

Fig. 3. A schematic view of the crystallographic structure of Sr_2NiUO_6 approximately along the *b*-axis. Large spheres represent Sr; corner-sharing NiO_6 (dark) and UO_6 octahedra are slightly tilted in order to optimize Sr–O bond-lengths.

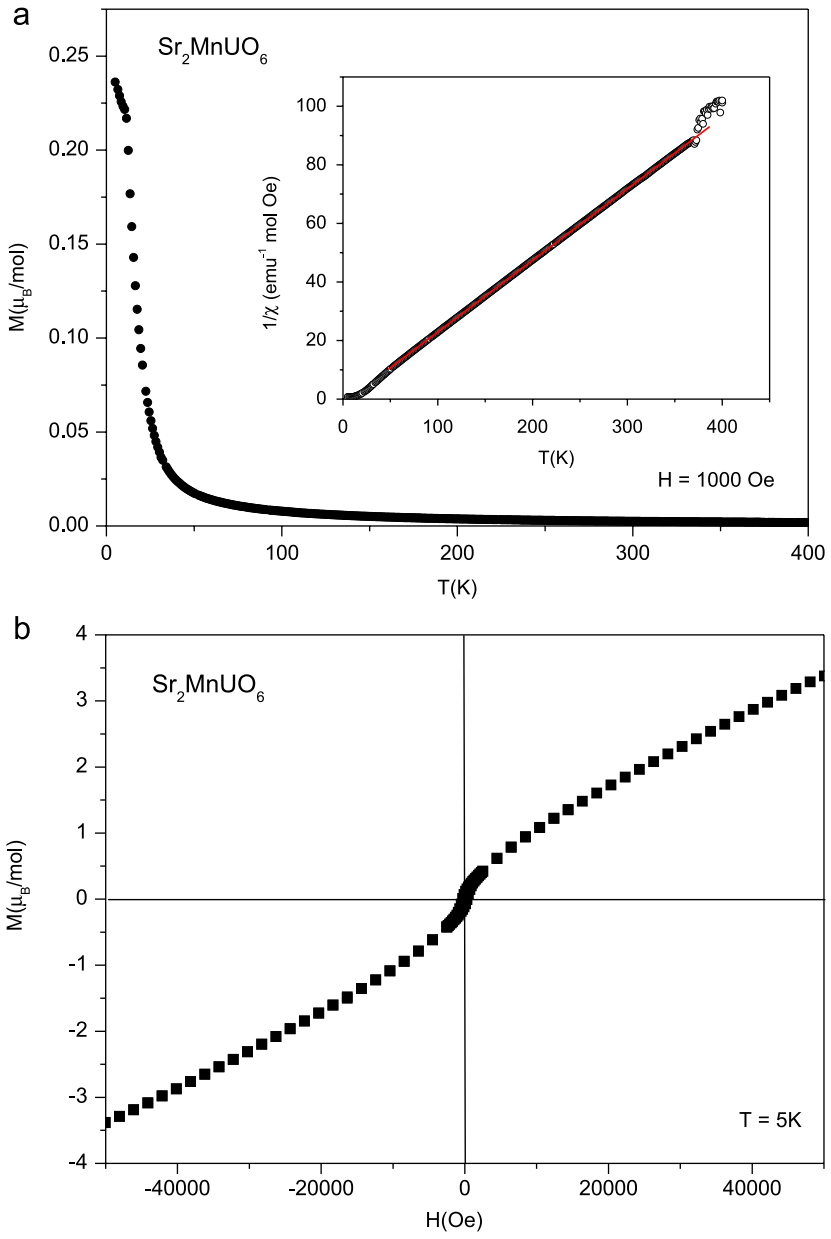

Fig. 4. (a) Magnetic susceptibility and (inset) reciprocal susceptibility for Sr_2MnUO_6; (b) magnetization isotherm at 5 K.

Zn^{2+} cation (2.14 Å), however for $B' =$ Mn, Fe and Ni the average distances to oxygen atoms ($\langle$Mn–O$\rangle = 2.07$ Å, $\langle$Fe–O$\rangle = 2.00$ Å and $\langle$Ni–O$\rangle = 2.03$ Å) are considerably smaller than those expected for high-spin $^{VI}Mn^{2+}$ (2.23 Å), $^{VI}Fe^{2+}$ (2.18 Å) and $^{VI}Ni^{2+}$ (2.09 Å): we suggest that the electronic configurations $Mn^{2+}U^{6+}$, $Fe^{2+}U^{6+}$ and $Ni^{2+}U^{6+}$ for these double perovskites could be considerably shifted towards $Mn^{3+}U^{5+}$, $Fe^{3+}U^{5+}$ and $Ni^{3+}U^{5+}$, respectively, since for high-spin hexacoordinated Mn^{3+}, Fe^{3+} and Ni^{3+} the expected B'–O distances are 2.05 Å, 2.04 Å and 2.00 Å, respectively. The average $\langle U$–O$\rangle$ bond-lengths range from 2.10 Å ($B' =$ Fe) to 2.18 Å ($B' =$ Mn), in acceptable agreement with the expected value for both U^{6+}–O (2.13 Å) or U^{5+}–O (2.16 Å) configurations.

3.2. Magnetic measurements

The variation of the magnetic susceptibility with temperature is shown in Figs. 4(a), 5(a) and 6(a) for $B' =$ Mn, Fe and Ni phases, respectively. On decreasing temperature, a noticeable increase in the susceptibility takes place below $T_N \approx 21$ K for Mn and Ni compounds, indicating the onset of a spontaneous magnetic ordering. For $B' =$ Fe, the magnetic ordering temperature is $T_C = 150$ K. The inset of Fig. 4 and 6 show that the inverse of the susceptibility presents a linear behavior at high temperature for Mn and Ni phases. A fit to a Curie–Weiss law in the temperature interval $76 < T < 358$ K ($B' =$ Mn) and $220 < T < 394$ K ($B' =$ Ni) gives a characteristic paramagnetic temperature $\Theta_W = 6$ K and

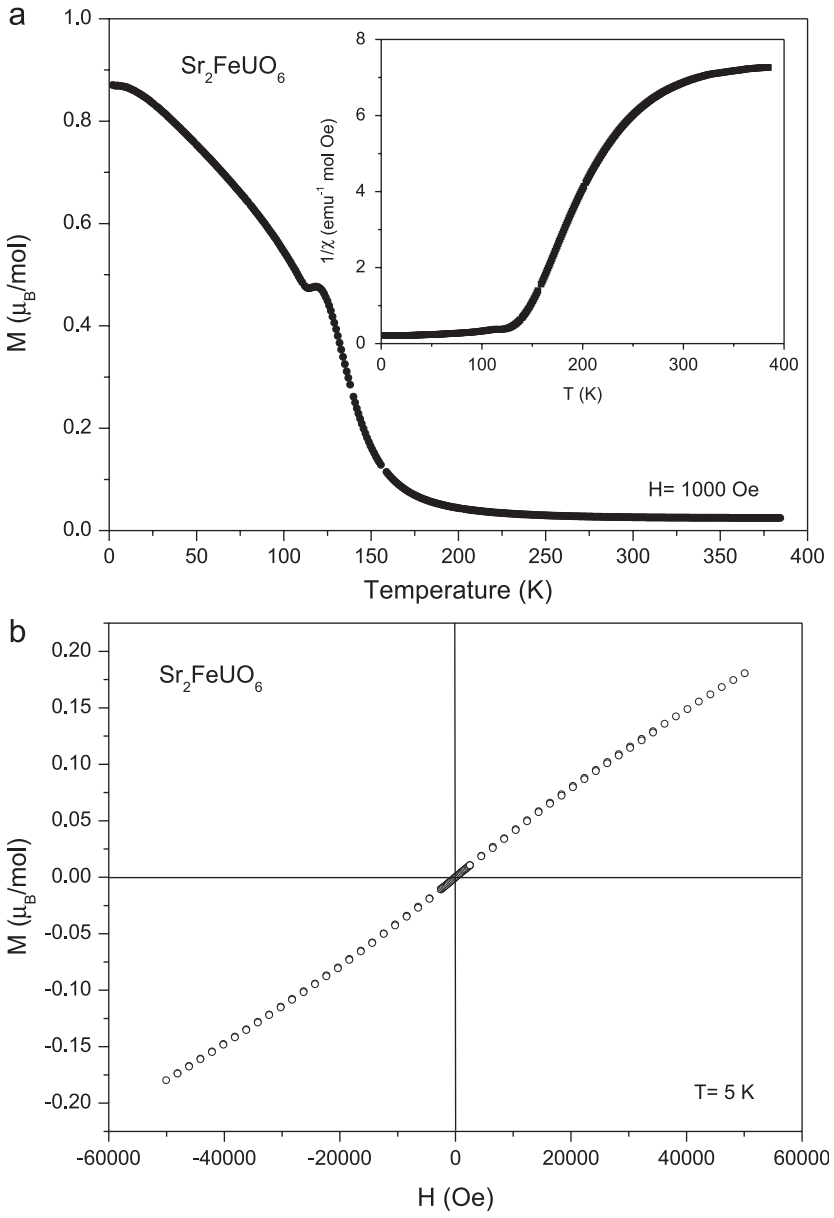

Fig. 5. (a) Magnetic susceptibility and (inset) reciprocal susceptibility for Sr_2FeUO_6; (b) magnetization isotherm at 5 K.

$\Theta_W = -21.5$ K for Mn and Ni compounds, respectively. The effective paramagnetic moment obtained from the Curie–Weiss fit for the Mn phase (5.74 μ_B/f.u.) is intermediate between those expected for high-spin Mn^{2+} (5.91 μ_B/f.u. for *spin-only* Mn^{2+}, $S = \frac{5}{2}$) in a Mn^{2+}–U^{6+} scenario, and 5.2 μ_B/f.u. for a Mn^{3+}(high spin, $S = 2$)–U^{5+}($S = \frac{1}{2}$) configuration, suggesting an intermediate situation for the perovskite Sr_2MnUO_6, as discussed from the ⟨Mn–O⟩ bond lengths. The slightly positive Weiss temperature ($\Theta_W = 6$ K) indicates a predominance of ferromagnetic interactions, also manifested in the magnetization vs. magnetic field curve (Fig. 4b), showing a remnant moment of 0.5 μ_B and a high-field magnetization up to 3.2 μ_B/f.u. for the maximum field of 5 T. For Sr_2NiUO_6 the effective paramagnetic moment is 3.51 μ_B/f.u., significantly higher than that expected for *spin-only* Ni^{2+} ($S = 1$) of 2.83 μ_B. As suggested for the Mn phase, it is possible to hypothesize on the presence of a partial internal disproportionation effect of the type $Ni^{2+} + U^{6+} \leftrightarrow Ni^{3+} + U^{5+}$, being 4.24 μ_B the expected moment for the configuration Ni^{3+}(high-spin, $S = \frac{3}{2}$)–U^{5+}($S = \frac{1}{2}$). At the same time, this charge disproportionation effect would account for the weak ferrimagnetic behavior observed in the magnetization curve (Fig. 6b), ascribable to a coupling between both $Ni^{2+/3+}$ and $U^{5+/6+}$ magnetic sublattices. The suggested ferrimagnetic interactions in Sr_2NiUO_6 would explain the negative Weiss temperature ($\Theta_W = -21.5$ K), the curvature of the reciprocal susceptibility and the presence of the characteristic shape of the magnetization in the low-temperature isotherm (Fig. 6b). Notice that the high-field saturation reached at 5 T is close to the 2 μ_B/f.u. expected for a perfect

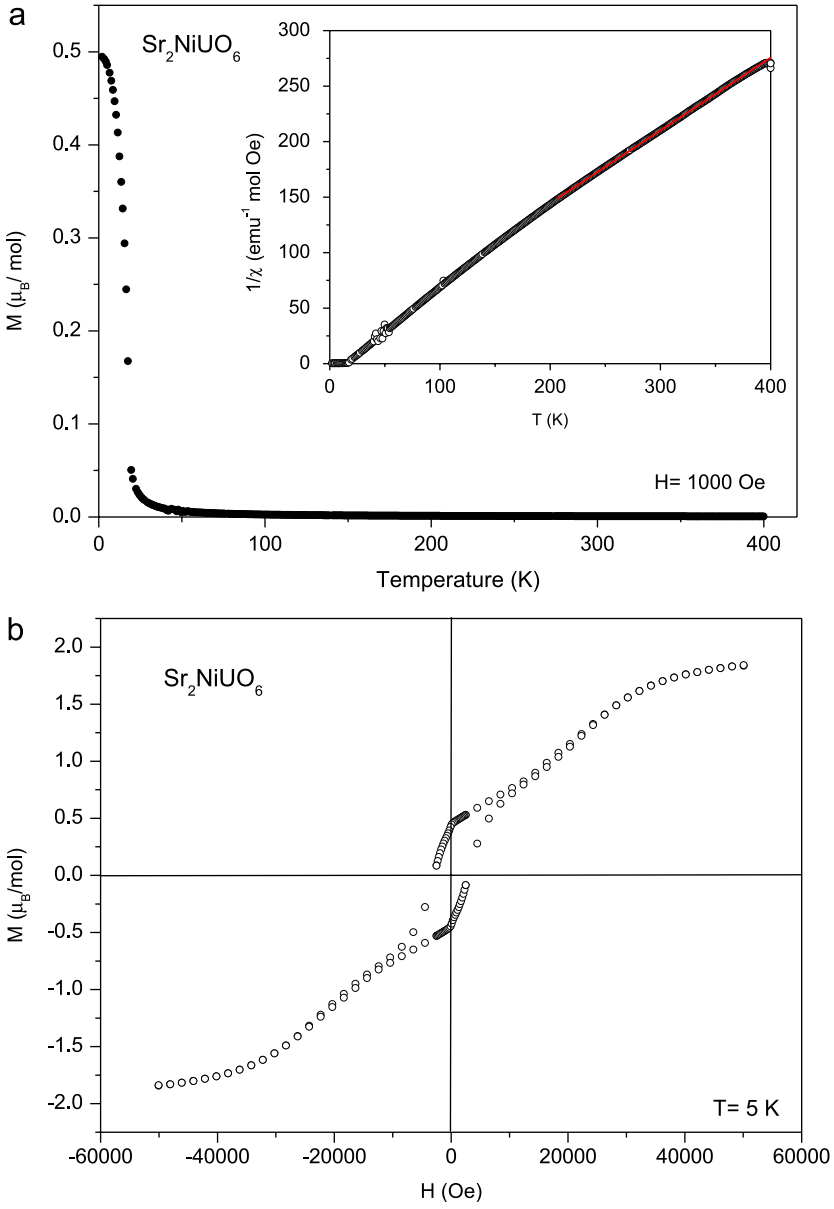

Fig. 6. (a) Magnetic susceptibility and (inset) reciprocal susceptibility for Sr_2NiUO_6; (b) magnetization isotherm at 5 K.

ferrimagnetic ordering between high-spin Ni^{3+} ($S=\frac{3}{2}$) and U^{5+} ($S=\frac{1}{2}$). This effect is strengthened in the Fe phase (Fig. 5), where the non-linearity of the reciprocal susceptibility is strongly marked and presents a huge curvature at temperatures above T_C, characteristic of ferrimagnetic interactions at high temperatures, precluding a Curie–Weiss fit in the available temperature range. With the present data it is not possible to find out the origin of the anomaly observed at 125 K; the microscopic origin of the magnetic behavior of the three phases will be the topic of a future study by neutron diffraction.

4. Conclusions

Four new double perovskites of composition $Sr_2B'UO_6$ (B' = Mn, Fe, Ni, Zn) have been prepared by thermal treatment either in air (Ni, Zn) or under reducing conditions (Mn, Fe). The crystal structure is monoclinic (space group $P2_1/n$); the crystal contains alternating $B'O_6$ and UO_6 octahedra, tilted along the three pseudo-cubic axes according to the Glazer notation $a^-a^-b^+$, as shown from XRD data. The B'–O distances obtained in the structural study suggest the presence of a partial disproportionation of the type $B'^{2+}+U^{6+} \Leftrightarrow B'^{3+}+U^{5+}$ for Fe, Mn and Ni cations; the same effect is confirmed from the Curie–Weiss fits to the reciprocal susceptibility for B' = Mn and Ni , since the observed effective paramagnetic moments are significantly higher (B' = Ni) or lower (B' = Mn) than expected for the spin-only divalent cations. The Fe perovskite shows a spontaneous magnetic ordering at relatively high temperatures of 150 K; the strong curvature observed in the reciprocal

susceptibility curve suggests the presence of ferrimagnetic interactions.

Acknowledgments

We thank the financial support of CICyT to the project MAT2004-0479 and of CAM to GR/MAT/0427/2004, and we are grateful to ILL for making all facilities available. R.E.C. thanks financial support from ANPCYT (PICT2003 06-15102), CONICET (PIP no. 5767) and SECyT-UNC (197/05). J.C.P. acknowledge the financial support of the CONICET (PIP 02482) and CyT (Universidad Nacional de San Luis-project 7707). J.C. Pedregosa and R.E. Carbonio are members of CONICET. We thank financial support provided by a CSIC-CONICET collaboration project.

References

[1] A.P.J. Ramirez, Phys.: Condens. Matter 9 (1997) 8171.
[2] C.N.R. Rao, B Raveau (Eds.), Colossal Magnetoresistance and other Related Properties in 3d Oxides, World Scientific, Singapore, 1998.
[3] K.-I. Kobayashi, T. Kimura, H. Sawada, K. Terakura, Y. Tokura, Nature 395 (1998) 677.
[4] A. Maignan, B. Raveau, C. Martin, M. Hervieu, J. Solid State Chem. 144 (1999) 224.
[5] K.-I. Kobayashi, T. Kimura, Y. Tomioka, H. Sawada, K. Terakura, Y. Tokura, Phys. Rev. B 59 (1999) 11159.
[6] J.A. Alonso, M.T. Casais, M.J. Martínez-Lope, J.L. Martínez, P. Velasco, A. Muñoz, M.T. Fernández Díaz, Chem. Mater. 12 (2000) 161.
[7] M.C. Viola, M.J. Martínez-Lope, J.A. Alonso, P. Velasco, J.L. Martínez, J.C. Pedregosa, R.E. Carbonio, M.T. Fernández-Díaz, Chem. Mater. 14 (2002) 812.
[8] M.C. Viola, M.J. Martínez-Lope, J.A. Alonso, J.L. Martínez, J.M. De Paoli, S. Pagola, J.C. Pedregosa, M.T. Fernández-Díaz, R.E. Carbonio, Chem. Mater. 15 (2003) 1655.
[9] M.S. Augsburger, M.C. Viola, J.C. Pedregosa, A. Muñoz, J.A. Alonso, R.E. Carbonio, J. Mater. Chem. 15 (2005) 2.
[10] R.D. Sánchez, D. Niebieskikwiat, A. Caneiro, L. Morales, M. Vásquez-Mansilla, F. Rivadulla, L.E. Hueso, J. Magn. Magn. Mater. 226 (2001) 895.
[11] M.S. Moreno, J.E. Gayone, M. Abbate, A. Caneiro, D. Niebieskikwiat, R.D. Sánchez, A. de Siervo, R. Landers, G. Zampieri, Solid State Commun. 120 (2001) 161.
[12] S. Nakamura, K. Ikezaki, N. Nakagawa, Y.J. Shan, M. Tanaka M., Hyperfine Interact 141 (2002) 207.
[13] S. Nakamura, M. Tanaka, H. Kato, Y. Tokura, J. Phys. Soc. Jpn. 72 (2003) 424.
[14] A. K Azad, S.G. Eriksson, A. Mellergard, S.A. Ivanov, J. Eriksen, H. Rundlöf, Mater. Res. Bull. 37 (2002) 1997.
[15] A.K. Eriksson, S.G. Eriksson, S.A. Ivanov, C.S. Knee, J. Eriksen, H. Rundlöf, M. Tseggai, Mater. Res. Bull. 41 (2006) 144.
[16] I.A. Ivanov, S.G. Eriksson, R. Tellgren, H. Rundlöf, M. Tseggai, Mater. Res. Bull. 40 (2005) 840.
[17] A.K. Azad, S.A. Ivanov, S.G. Ericsson, J. Eriksen, H. Rundlöf, R. Mathiev, P. Svedlindh, Mater. Res. Bull. 36 (2001) 2485.
[18] A.K. Azad, S.A. Ivanov, S.G. Ericsson, J. Eriksen, H. Rundlöf, R. Mathiev, P. Svedlindh, Mater. Res. Bull. 36 (2001) 2215.
[19] A.K. Azad, S.A. Ivanov, S.G. Ericsson, H. Rundlöf, J. Eriksen, R. Mathiev, P. Svedlindh, J. Magn. Magn. Mater. 237 (2001) 124.
[20] A.K. Azad, S.G. Ericsson, Solid State Commun. 126 (2003) 503.
[21] A.K. Azad, S.G. Ericsson, S.A. Ivanov, R. Mathiev, P. Svedlindh, J. Eriksen, H. Rundlöf, J. Alloys Compounds 364 (2004) 77.
[22] P. Leporcher, G. André, T. Roisnel, T. Le Bihan, H. Noël, J. Alloys Compounds 213–214 (1994) 506.
[23] Y. Hinatsu, J. Alloys Compounds 215 (1994) 161.
[24] Y. Hinatsu, J. Solid State Chem. 105 (1993) 100.
[25] Y. Hinatsu, Y. Doi, J. Solid State Chem. 179 (2006) 2084.
[26] R. Pinacca, M.C. Viola, J.C. Pedregosa, A. Muñoz, J.A. Alonso, J.L. Martínez, R.E. Carbonio, Dalton Trans. (2005) 447.
[27] H.M. Rietveld, J. Appl. Crystallogr. 2 (1969) 65.
[28] J. Rodríguez-Carvajal, Physica B 192 (1993) 55.
[29] P.M. Woodward, Acta Crystalogr. B 53 (1997) 32.
[30] R.D. Shannon, Acta Crystallogr. Sect. A 32 (1976) 751.